

A discussion about inelastic surface scattering

H. J. LAUTER^{†*} and V. LAUTER-PASYUK^{‡¶}

[†]Institut Laue Langevin, BP 156, F-38042, Grenoble Cedex 9, France

[‡]Physik Department, TU München, D-85747 Garching, Germany

[¶]Joint Institute for Nuclear Research, 141980, Dubna, Moscow Region, Russia

(Received 5 January 2005; revised 21 March 2005; in final form 21 April 2005)

A study is presented in which spin waves were measured in reflection geometry in a supermirror multilayer. The existence of spin waves is proven by the cut-off of spin wave scattering. By analogy with off-specular scattering it is worked out how perturbation theory has to be applied to inelastic surface scattering (ISS). Through interference effects mainly of a multilayer, but also of scattering in the total reflecting region, appreciable intensity can be gained so that we predict that more detailed studies of spin waves will become possible. The encoding of the angle and of the wavelength using Larmor precession will greatly help to separate inelastic scattering from other scattering contributions.

Keywords: Inelastic Scattering; Surface Phonons; Spin Waves; Multilayer

1. Introduction

Inelastic neutron scattering from surfaces is still a challenge. The main reason is that the number of scattering centers in a surface is small and that neutron scattering is a weak interaction. Here we will present a first experiment about spin-wave excitation in a supermirror film using the reflection geometry. The reflection geometry, which will be discussed, can render inelastic neutron scattering sensitive to surface layers.

In a first train of thoughts inelastic scattering can become surface sensitive when the role of the structure factor of a Bragg peak in the inelastic scattering [1] is replaced by a momentum transfer of the reflectivity curve, e.g. the critical reflection. The usual picture for introduction to inelastic scattering is shown in figure 1. Here the momentum transfer \mathbf{Q}_z perpendicular to the surface of a sample replaces the reciprocal lattice vector $\mathbf{Q}_{\mathbf{hkl}}$ of a bulk sample. It is not evident how this choice can lead to a higher scattering intensity. However, the scattering process shown in figure 1 is too simple, perturbation theory has to be used for inelastic surface scattering (ISS) in reflection geometry. This theory is not yet developed for ISS but by analogy with off-specular scattering [2] some conclusions will be drawn. In particular, it will become evident why an appreciable increase in intensity will be obtained in reflection geometry through interference effects. A further increase of intensity is obtained through the incoming scattering angle α_i and so an appreciably bigger footprint of the sample compared to the real thickness of a surface layer or of a multilayer. The number of layers of a multilayer

*Corresponding author. Email: lauter@ill.fr

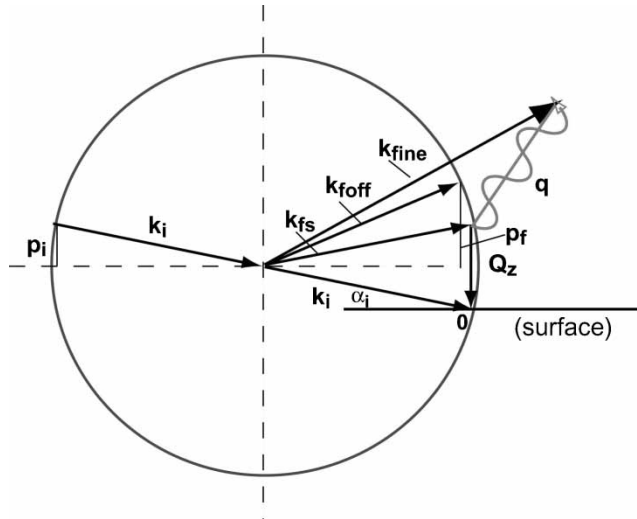


Figure 1. Diagram in reciprocal space for phonon scattering at a surface with \mathbf{Q}_z the momentum transfer perpendicular to the surface. \mathbf{k}_i , \mathbf{k}_{fs} , \mathbf{k}_{off} and \mathbf{k}_{fine} mark the wave vector of the incoming neutrons and scattered neutrons for specular scattering, off-specular scattering and inelastic scattering, respectively. \mathbf{p}_i and \mathbf{p}_f are the surface components perpendicular to the wavevectors, here given for off-specular scattering. \mathbf{q} is the phonon momentum.

will of course also contribute to an increase of intensity. However, there are still ~ 2 orders of magnitude of intensity between the geometry in reflectometry and the geometry in transmission with a 90° turned sample. It will be shown that interference effects, taken into account by the perturbation theory, will compensate this factor.

The term $(\boldsymbol{\kappa} \cdot \mathbf{e}_s)^2$ in the coherent scattering cross section, with $\boldsymbol{\kappa} = \mathbf{k}_i - \mathbf{k}_{fine}$ (see figure 1) and \mathbf{e}_s the polarization vector of a normal mode s , gives the polarization of the phonon [1]. Thus the phonon shown in figure 1 has more longitudinal character, if \mathbf{e}_s is assumed to be parallel to \mathbf{Q}_z . This shows that phonons with different polarization can also be measured at a surface. In addition, if \mathbf{Q}_z will be associated to the inelastic scattering through perturbation theory, then it will be shown that the scattering is depth sensitive which is a tool particularly important for a layered structure. The use of reflectivity can create (or annihilate) phonons with propagation along the surface with perpendicular polarization and also phonons with propagation perpendicular to the surface with longitudinal polarization as can be easily verified from the scheme in figure 1. In order to investigate the not yet mentioned polarization directions of the phonons, the momentum transfer vector must be turned along the surface and the sample should be turned by 90° . But then we are no longer in reflection geometry. The 2-fold symmetry of the surface creates this effect. The previous considerations are true only if we have in reflection geometry no reflected wave from the interfaces inside the sample but only a wave being transmitted through the sample at grazing incidence.

The inclusion of the reflected waves into the considerations of ISS leads to perturbation theory and is outlined after the experimental part, in which a study of spin-waves in thin layers is presented. Finally, it will be discussed how GISANS scattering can be separated from ISS and intensity be enhanced with angular encoding.

2. Surfaces spin-waves

Surface spin-waves [3] are a hot topic in view of nano-technology [4], and neutron scattering is predestined to investigate their behaviour. Neutron scattering has given much information

in studies of bulk matter, however, there is a lack of information about surface magnons studied with neutrons. Other methods like Brillouin scattering or ferromagnetic resonance have given information about the magnetic surface excitations around the centre of the Brillouin zone. Recently spin-polarized electron energy loss spectroscopy (SPEELS) applied to a thin film was able to explore the high energy and high wave vector spin-wave region [5].

A first result with neutron scattering on a relatively thick multilayer film was obtained with neutron inelastic scattering [6], but 350 bilayers were necessary to get some scattered intensity. Here we want to report about an experiment, in which reflection geometry was used to determine the stiffness constant of a FeCo/TiZr supermirror on a glass-substrate [7,8]. Prior to the presentation of the reflectometry experiment on spin-waves, the experiment on bulk amorphous Fe–Ni-based ferromagnets is given [9,10], which serves as comparison to the film experiment.

In small-angle polarized neutron scattering (SAPNS) applied to an isotropic ferromagnet, a cut-off of the scattered intensity appears at the scattering angle θ_0 [11,12], which is related to the stiffness constant of the spin-waves by $\theta_0 = 1/\alpha = \hbar^2/2Dm_n$ with the stiffness constant D from the dispersion relation $\omega_q = Dq^2$ and α the ratio of the neutron mass to the effective mass of the spin-wave. ϵ_q is the energy of the spin-wave and \mathbf{q} , $q = |\mathbf{q}|$, the spin-wave wave vector. This result is an approximation in the limit of $\alpha \gg 1$, obtained when energy and momentum conservation law are brought together under the assumption of the quadratic dispersion law for spin-waves, which is valid in an isotropic ferromagnet for small momentum transfer. The graphical solution is presented in figure 2 exhibiting the cut-off angle Θ_0 when $\mathbf{k}_{f+} = \mathbf{k}_f$ (\mathbf{k}_{f+} and \mathbf{k}_f are the wave vectors for energy gain and energy loss, respectively).

In figure 3 the SAPNS intensity of the investigated ferromagnet is shown and the cut-off angle θ_0 is marked. This cut-off is the edge of the “density of states of the spin waves” (see figure 2) and thus visible without energy analysis. It should be noted that the directional relation between the momentum transfer \mathbf{q} and the magnetization \mathbf{m} in the SAPNS magnetic scattering cross-section gives, under certain conditions of the set-up of the experiment [9,10], an antisymmetry of the scattered intensity with respect to both the polarization P° and the scattering angle θ , as easily seen in figure 3.

The previously described experiment has been repeated with a supermirror multilayer as a quasi 2-dimensional example [7,8]. The idea was to get a proof of inelastic scattering from a thin sample surface measured in reflection geometry without energy analysis; indeed the cut-off angle in figure 3 provides such an effect.

A monochromatic beam impinges under the critical angle γ of the multilayer onto the sample and is specularly reflected in the horizontal scattering plane (figure 4). The recorded

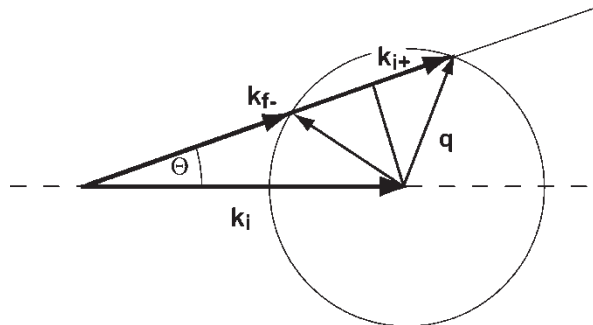


Figure 2. Diagram of kinematic neutron scattering from a spin-wave in an amorphous ferromagnet (quadratic dispersion). The maximal \mathbf{q} -vector is obtained for $\mathbf{k}_f = \mathbf{k}_{f+}$, which relates to the cut-off angle Θ_0 .

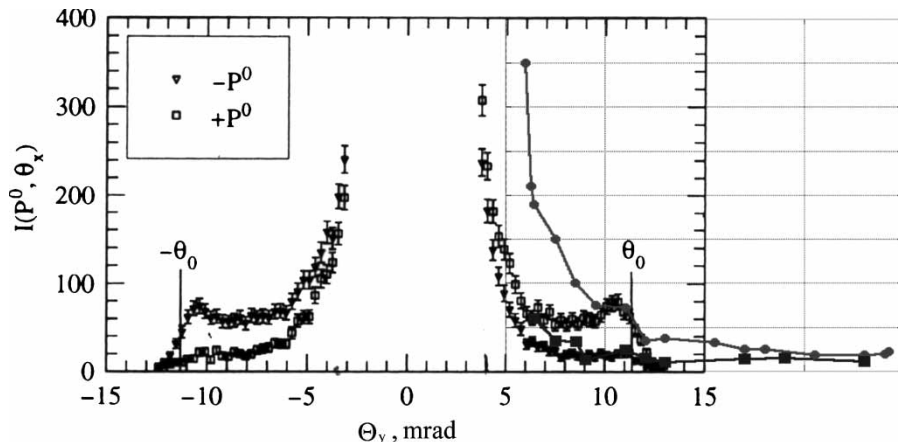


Figure 3. SAPNS intensity as a function of the scattering angle for + and - polarization P^0 (black squares and triangles) [11,12]. The results of [9] have been imported and marked in red and blue for the different polarizations.

inelastic scattering is obtained by scanning the Cd-slit in the perpendicular plane along the y -direction in front of the detector as a function of the angle θ . Thus specular reflection and inelastic scattering are separated (outside the overlapping region given by the finite resolution) having momentum transfer vectors in different directions. The reflection geometry serves also to enhance the inelastic scattered signal due to the fact that the footprint of the sample is at least 4 orders of magnitude bigger than the film thickness. The inelastic scattering in the y -direction (see figure 4) is compared to the bulk SAPNS scattering in the previously described experiment (see figure 3). The ordinate of the diagram in the original publication [8] has been changed to a logarithmic scale [9,10] and the intensity has been scaled. Again a cut-off angle is detected and also with an asymmetry with respect to the polarization P^0 . The discussion of the fact that the cut-off angle is nearly the same as for the sample in bulk SAPNS-experiment and thus that the same stiffness constant was obtained, is not within the scope of this article.

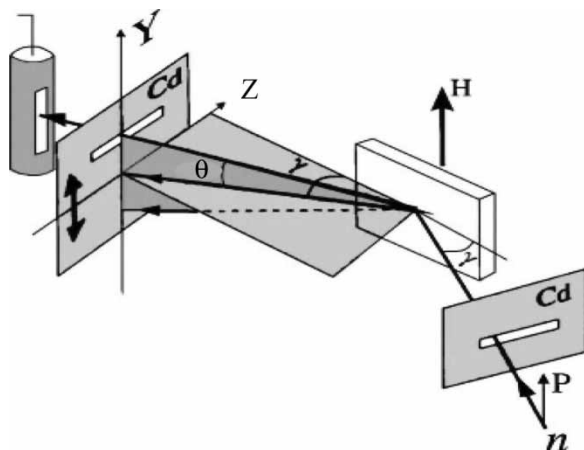


Figure 4. Experimental set-up to demonstrate spin-wave scattering in a supermirror multilayer in reflection geometry without energy analysis from [9]. H is the magnetic field to magnetize the sample. The set-up is described in the text.

In a model without interference effects in the multilayer a spin-wave is excited with transverse polarization traveling along the surface direction (y-direction in figure 4). The main result is that, in reflection geometry enough intensity is collected, so that phonons can be studied in thin layers in ISS. The experimental set-up can be improved even more because a monochromatic beam has been used at the pulsed reactor IBR-2 at Dubna [13]. A complete TOF set-up at the IBR2 or a monochromatic spectrometer at a high flux reactor will certainly allow spin-waves of single thin layers to be studied in more detail.

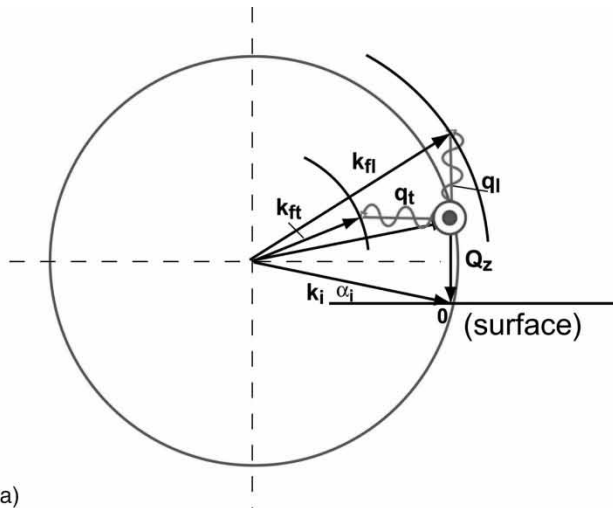
3. Surface phonons and off-specular scattering

In this section, we describe the application of perturbation theory to surface phonon excitations and underline the effect of an unperturbed wave field in, e.g. a multilayer on the intensity of the phonon excitation by model calculations for off-specular scattering.

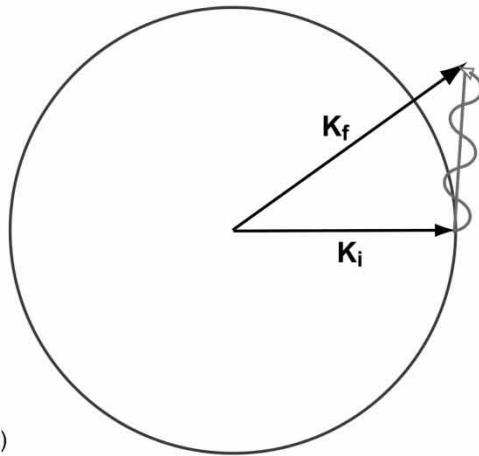
The scattering geometry of the previous experiment (see figure 4) is shown in reciprocal space in figure 5a for the discussion of a more correct approach to inelastic scattering from a surface. The phonons have a direction of propagation perpendicular and parallel to the surface, with longitudinal and transverse polarization (this simplified picture is valid under the assumption of $\mathbf{Q}_z \ll \mathbf{k}_i - \mathbf{k}_f$). The process of phonon absorption and phonon creation will happen, respectively, according to the relative magnitude of \mathbf{k}_i with respect to \mathbf{k}_f . In the experimental set-up shown in figure 4 the transverse phonon is perpendicular to the scattering plane of $(\mathbf{k}_i, \mathbf{k}_f)$ and is represented by the circles in figure 5a. In the phonon expansion [1] two processes, the elastic scattering at a Bragg peak \mathbf{Q}_{hkl} and the inelastic process with the momentum of the longitudinal or transverse phonon with \mathbf{k}_{fl} and \mathbf{k}_{ft} , respectively, are treated in the kinematic approximation [1]. This means that the reflection of neutrons from interfaces or the substrate is not included. Here, the procedure of perturbation theory has to be applied also taking into account dynamical effects due to multiple scattering. This theory is known as the distorted wave born approximation (DWBA) [14]. An equivalent procedure for surface phonon scattering has not yet been developed but can be outlined.

First the neutron wavefield has to be calculated inside the sample, for example a multilayer, to be probed for surface phonons. This wavefield is built up by all reflected and transmitted waves inside the sample. The transfer towards the detector of the neutrons from this wavefield through the sample interfaces results in the specular line along $\mathbf{Q}_z(\alpha_i)$ under the condition $\alpha_i = \alpha_f$ (α_i is the incoming angle of \mathbf{k}_i with respect to the sample surface (see figure 1) and α_f the outgoing angle). As an example we show in figure 6a the reflectivity of an $[\text{Fe}/\text{Cr}]_{\times 12}$ multilayer [15] to which the DWBA [2] has been successfully applied. The specular line is the vertical line at $p_i = p_f$. If perturbations, in this case magnetic domains, are present inside the unperturbed wavefield, then (small angle-)scattering is caused by the perturbations and is transmitted through the multilayer interfaces towards the detector as for the case of off-specular scattering. In the example in figure 6a all kinds of off-specular scattering are detected such as Yoneda-scattering and Bragg-sheet scattering, including Yoneda scattering from different “critical angles” or Bragg-sheet scattering from total thickness oscillations [15]. These are effects originating from high intensity transmission at “critical potentials” and from high amplitude modulations in the undistorted wavefield. Also the magnetic structure plays an important role leading, in the example of figure 6a, to non-spin flip scattering on the reflectivity curve, and to spin flip scattering of the off-specular scattering [15], which are not separated in figure 6a.

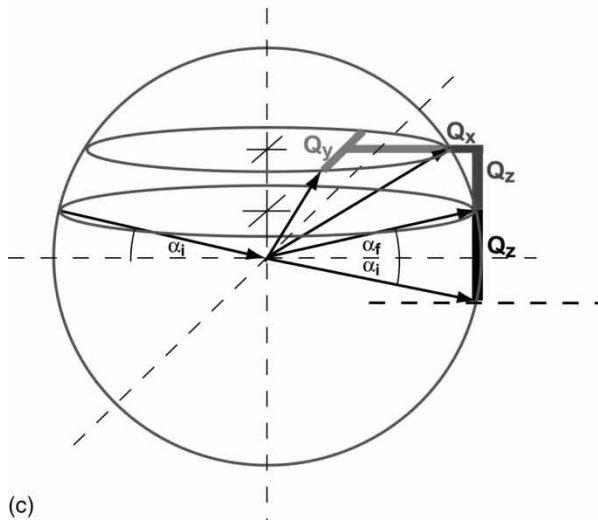
In figure 6b the sample composition has been changed to a Cr/Fe/Cr/substrate multilayer with a low potential of the substrate layer. The calculated off-specular scattering has drastically changed with respect to the figure 6a. The Bragg-sheet scattering has disappeared



(a)



(b)



(c)

and the Yoneda scattering has considerably reduced due to the low substrate potential. The reduction in off-specular intensity reaches 3 orders of magnitude. By inverting the argument we can gain 3 orders of magnitude in off-specular intensity in adjusting critical angles and using multilayers. In particular the Bragg-sheet scattering is depth sensitive and one can adjust the incoming scattering angle α_i to provide a high intensity of the unperturbed wavefield at the location of the perturbations in the sample (or to layers in which phonons should be created).

Now we can try to transfer these findings to ISS. One clear fact is that the neutron wavefield has to be calculated first inside the multilayer sample. We have seen in off-specular scattering that a multilayer and a high substrate potential are tools to increase the wavefield inside the sample for certain incoming wave vectors. The second part is to calculate the ISS inside the sample with the given unperturbed wavefield and then to add all the transmission functions of the multilayer interfaces for inelastically scattered neutrons.

The scattering diagram has changed with the introduction of the interference effects in particular due to reflection at the substrate. In figure 5b a revised scattering diagram for the study depicted in figure 3 is shown taking into account only the scattering vectors inside the multilayer sample (dynamical scattering [1]). So, phonon scattering is performed with \mathbf{k}_i and \mathbf{k}_f being vectors inside the sample or, more precisely in the case of the Fe/Cr multilayer, inside one Fe-layer. Assuming ideal reflection at the substrate the incoming wave vector \mathbf{k}_i , created by the unperturbed wavefield, becomes parallel to the surface, which may not be true for all layers of the Fe/Cr multilayer or of the supermirror. But as a scan in the y -direction is performed (see figure 4) those magnons are selected from the polycrystalline sample, which fulfill the scattering conditions (see [9–11]) in this direction. It turns out that, through the introduction of the reflection at the substrate, the polarization of the magnon is longitudinal. Furthermore, the intensity increase due to scattering at the Bragg-peaks of the supermirror is included in the ISS through the increase of the amplitude of the unperturbed wave field inside the supermirror at certain incoming angles α_i . It seems easy to extend the above consideration to phonons of the multilayer structure itself, and therefore to vibrations of one layer with respect to neighboring layers, which we do not include in this article.

4. Separation of off-specular and surface phonon scattering

In figure 5c the scattering configuration of off-specular scattering and GISANS [16] scattering is shown. Comparing this with the various configurations of ISS in figure 5a, the conclusion can be drawn that an overlap between the two scattering features is very likely, because only in rare cases roughness and domains can be avoided. As an example the model calculation is shown in figure 6a for a sample with no measurable interface roughness but with magnetic domains [15]. It would be of advantage to look for ISS in TOF to get a better overview of the location of inelastic events due to the still rather unknown effects of the interface transmission functions on the inelastic scattering. A further help in TOF is given by the distinct separation of direct and reflected beam. Another way to distinguish the two signals without energy analysis is to use Larmor precession. This is discussed in the following for a TOF set-up.

Figure 5. (a) Phonons with direction of propagation perpendicular and parallel to the surface. The circles mark the second transverse phonon with propagation perpendicular to the drawn plane, which is the $y - z$ plane as in figure 4. (The transverse phonon is only transverse for a small \mathbf{Q}_x with respect to q_i). (b) Phonon inside the sample due to the momentum transfer $\mathbf{k}_i - \mathbf{k}_f$ with \mathbf{k}_i and \mathbf{k}_f defined inside the sample. (c) Specular scattering shown by \mathbf{Q}_z (black); off-specular scattering in \mathbf{Q}_x direction (violet) and GISANS in \mathbf{Q}_y direction (green).

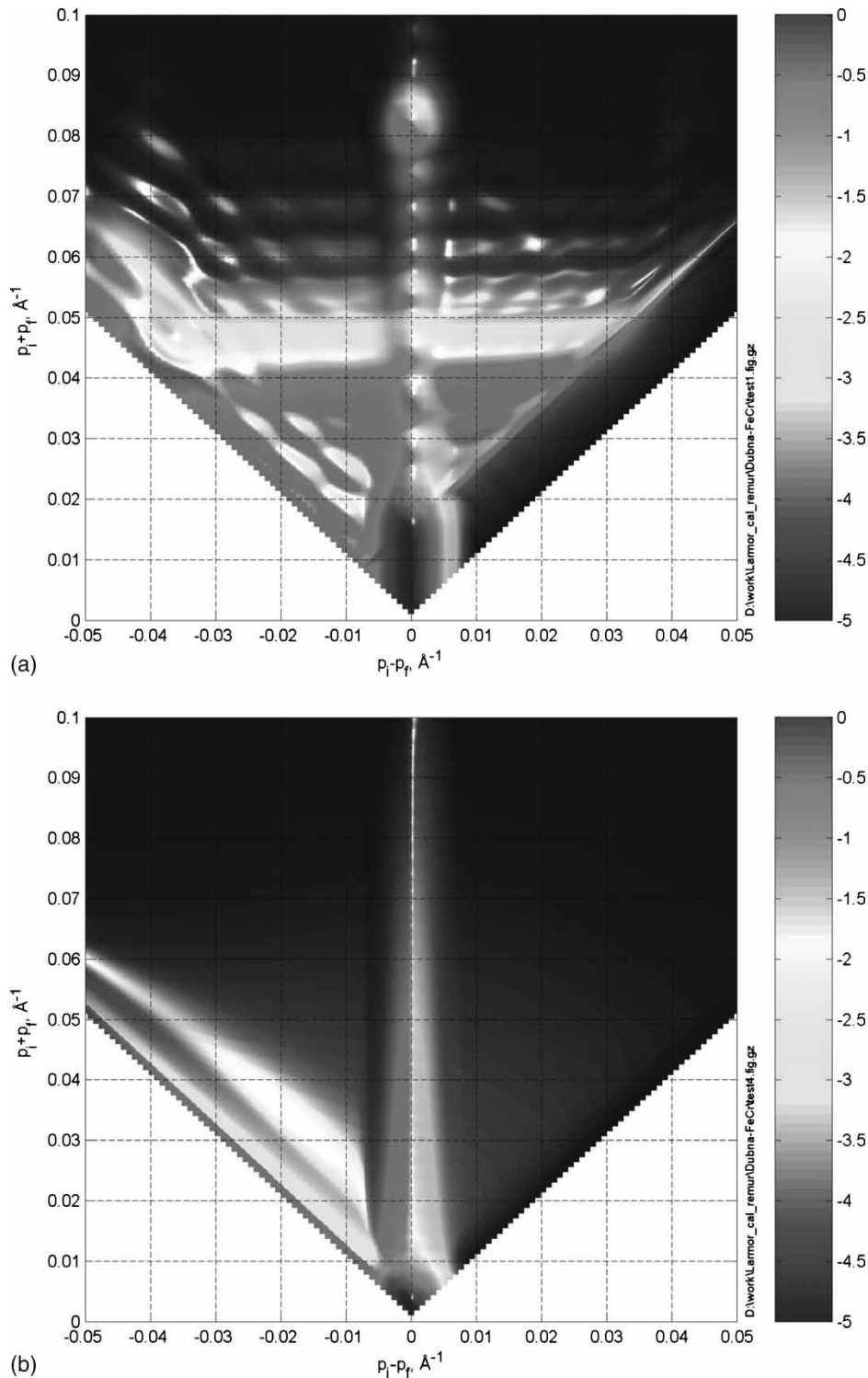
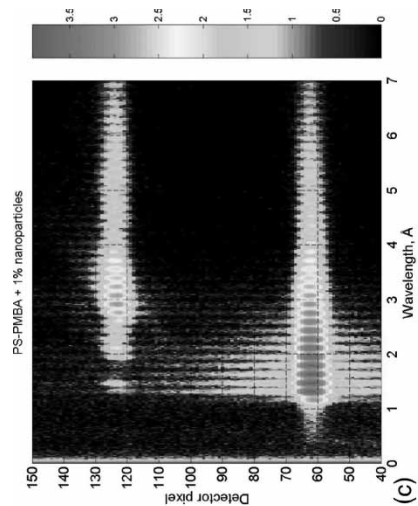
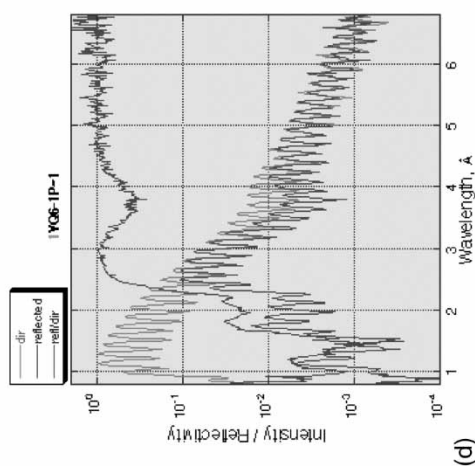


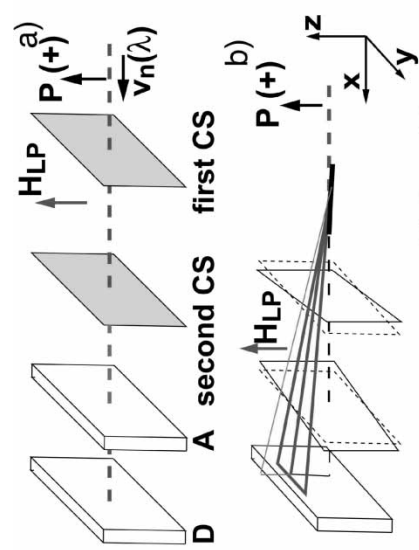
Figure 6. (a) Specular and off-specular scattering intensity maps from a Fe/Cr multilayer [17] as a function of $\mathbf{p}_i + \mathbf{p}_f = \mathbf{Q}_z$ and $\mathbf{p}_i - \mathbf{p}_f$; \mathbf{p}_i and \mathbf{p}_f are the components of the incoming and outgoing wavevector (see figure 1) perpendicular to the surface, so the specular line is along $\mathbf{p}_i - \mathbf{p}_f = 0$. (b) Specular and off-specular scattering intensity map from a Cr/Fe/Cr trilayer with reduced potential of the substrate with respect to figure 6a.



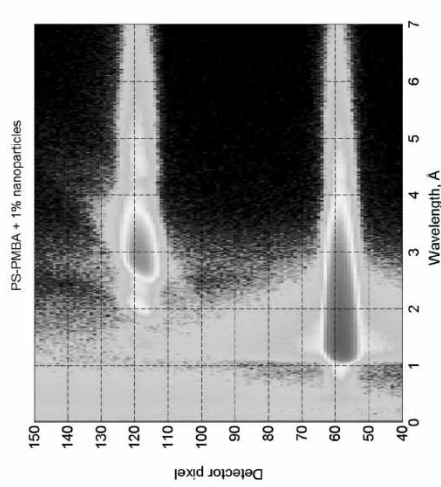
(c)



(d)



(a) D&A sample second CS first CS



(b)

We presented in [17] the encoding of wavelength using a set-up of two current sheets and neutrons from a pulsed source in TOF. The scheme of the experimental arrangement is shown in figure 7a with the experimental results in figure 7b–d. The incoming polarized beam shown in figure 7a is transformed by the first current sheet in a beam with neutrons, which are Larmor precessing around the magnetic field H_{LP} . The second current sheet serves “to turn the Larmor precession plane” perpendicular to the reflection plane of the analyzer, so that the phase of the Larmor precessing neutrons is analyzed. The phase of the neutrons is given by the field integral between the two current sheets [17]. If a sample is brought in front of the current sheets as shown in the lower part of figure 7a, then two intensity spots appear on the detector. One spot, the lower one, originates from the direct beam and the upper one from the reflected beam. Thus in time-of-flight they appear as demonstrated in figure 7b as two traces of intensity as a function of the detector pixel and the wavelength λ . The direct beam reflects the intensity distribution of the incoming neutrons as $f(\lambda)$. The 2-dimensional intensity map in figure 7b was taken with the current sheets switched off. The effect of the Larmor precession is magnificently demonstrated in figure 7c by the appearance of the intensity oscillations along the wavelength axis, and with a frequency independent of the wavelength [17]. In figure 7d a cut along the specular reflected beam and the direct beam from figure 7c is shown as a function of the wavelength. Both scans of course exhibit intensity oscillations. The normalization of the reflected beam by the direct beam leads to the third curve in figure 7d, in which the oscillations have disappeared. This proves that the Larmor frequency influences in the same way the reflected and the direct beam, but does not influence effects arising from the sample properties which are given by the reflectivity curve, the third curve in figure 7d.

However, this is not quite correct because the path length the neutrons travel between the two current sheets is slightly different for the direct and reflected beam (see figure 7a). A different oscillation frequency is expected, but the path length difference is so small that it can be neglected as long as the two current sheets are perpendicular to the direct beam direction. However, the sensitivity can be significantly enhanced if the current sheets are turned. The enhancement of this effect, which results in a higher phase shift between the direct and reflected beam directions can be used to perform angular encoding. This set-up is sketched in the lower scheme in figure 7a. Here the rotation of the current sheets is not made around the z -axis, thus it does not influence the scattering along the z -axis but it does influence the scattering along the y -axis. This means that either GISANS scattering (see figure 5c) or the transverse phonon in figure 5a can be encoded.

In addition to angular encoding which is sensitive to the angular variation in phonon scattering the change of energy of the neutron also contributes to a change of the phase of the oscillation frequency of the intensity (see figure 7c). As shown in figures 4 and 5a the inelastic scattering is assumed to be detected perpendicular to the elastic scattering at the critical edge, which is in figure 7d at $\mathbf{Q}_z = 4\pi \sin(\theta)/\lambda$, with $\lambda \sim 4.5 \text{ \AA}$. A scattering event without change of energy would appear as presented in figure 8a. The intensity of the phonon (circles in figure 5a) shows up perpendicular to the reflectivity line being encoded following

Figure 7. (a) Scheme for wavelength-encoding of a polarized white pulsed neutron beam. $v_n(\lambda)$ is the wavelength dependent neutron velocity, P the neutron polarization, H_{LP} the magnetic field between the current sheets CS, A the analyzer and D the detector. Lower part: Scheme for angular encoding with inclined current sheets and with a sample in reflection geometry. (b) Intensity map from scattering in the reflectometry set-up in figure 7a with current sheets inactive as a function of the detector pixel position and the wavelength λ . The sample is a polymer multilayer. (c) Intensity map from scattering in reflectometry set-up from figure 7a but with active current sheets. (d) Intensity traces from figure 7b along the direct beam (red) and the reflected beam (blue) as a function of the wavelength λ . The green curve is the reflectivity obtained by normalization of the reflected beam intensity to the direct beam intensity.

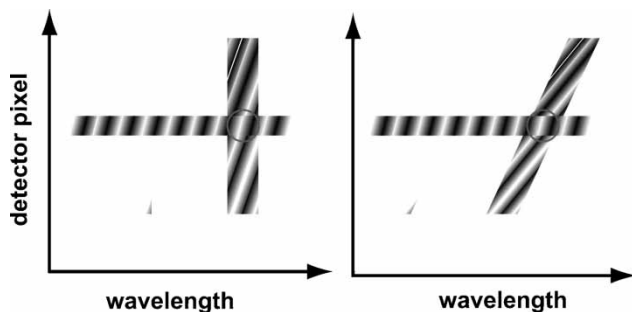


Figure 8. Schematic encoded intensity distribution for GISANS scattering in (a) and ISS in (b) as a function of the detector pixel position and the wavelength λ .

the idea of the turned current sheets in figure 7a with a consequently inclined axis of the Larmor precession oscillations. However, a loss in energy of the scattered neutron makes that the path of maximal intensity, which follows the dispersion curve, is inclined in the pixel- λ diagram and the phase of the oscillations are shifted as a function of energy loss (the shift is in opposite direction for energy gain). This effect is demonstrated schematically in figure 8b with an approximately linear dispersion. The intensity distribution in figure 8a could be interpreted as GISANS scattering that can be distinguished from the inelastic scattering due to the phase shift of the oscillation of the inelastic scattering. Thus even if the scattering in figure 8a overlaps with the scattering in figure 8b it can be separated out due to the wavelength (and angular) encoding. Without the extra effect of encoding, the separation of ISS with respect to GISANS would be not possible at small energy transfer.

A phase shift of the oscillations can also be obtained if a magnetic sample is put **inside** the Larmor oscillation region between the current sheets in figure 7a. The magnetic induction inside the sample (a Fe/Cr multilayer) creates a different local field integral and a phase shift of the Larmor precession neutrons is created. This effect has also been proven recently with an Fe-layer [18]. The phase shift is visualized by normalization of the reflected intensity to the direct beam intensity. Now oscillations appear along the reflectivity curve [17] whereas the same normalization procedure leads to the reflectivity curve of figure 7d without oscillation due to the fact that the sample was outside the Larmor precession region. The oscillations reflect the inner magnetic structure of the sample. The magnetic effect from the magnetic sample can be extracted from the data more easily if the encoding technique is employed. Thus also weak signals such as from ISS should become visible with the help of encoding, which is certainly also useful for discrimination against off-specular scattering.

A last remark concerns a modified set-up with the current sheets in front of the sample [17]. In this configuration a beam, which is converging onto the sample, is angular encoded. The reflected intensity, which under these conditions and without encoding would be smeared out on the detector, can be reconstituted with high angular resolution using angular encoding. This application of the encoding technique, which is equivalent to an appreciable increase in signal intensity, seems to be promising for low intensity signals or high-resolution studies.

5. Conclusions

In summary several aspects of surface phonons were discussed: (i) In reflection geometry the cut-off of the density of states of spin-waves was measured and thus surface spin-waves in a rather thin magnetic film demonstrated. (ii) The study of surface phonon scattering is depth

sensitive and requires perturbation theory and dynamical theory. (iii) Intensities of off-specular scattering and inelastic surfaces scattering may overlap. (iv) Angular and wavelength encoding is necessary to extract ISS from the other scattering contributions. In the monochromatic mode the encoding can be used without energy analysis to deduce the dispersion curves of surface phonons.

Acknowledgements

Helpful discussions with B. Toperverg, V. Bodnarchuk and T. Gutberlet and the support of the German Ministry BMBF are acknowledged (Project: 03DU03MU).

References

- [1] G.L. Squires, *Thermal Neutron Scattering* (Cambridge University Press, 1978); W. Marshall and S.W. Lovesey, *Theory of Thermal Neutron Scattering* (Oxford Clarendon Press, 1978).
- [2] B.P. Toperverg, *Physica B* **297** 160 (2001); B.P. Toperverg, O. Nikonov, V. Lauter-Pasyuk, H.J. Lauter, *Physica B* **297**, 169 (2001).
- [3] D.L. Mills, Surface spin waves on magnetic crystals. in *Surface Excitations*, edited by V.M. Agranovich and R. Loudon (Elsevier Science Publisher, 1984).
- [4] B. Hennion, *Phys. Rev. B* **66** 224426 (2002).
- [5] R. Vollmer, M. Etzkorn, P.S. Anil Kumar, H. Ibach, J. Kirschner, *Phys. Rev. Lett.* **91** 147201 (2003).
- [6] A. Schreyer, T. Schmitte, R. Siebrecht, P. Bödeker, H. Zabel, S.H. Lee, R.W. Erwin, C.F. Majkrzak, J. Kwo and M. Hong, *J. Appl. Phys.* **87** 5443 (2000).
- [7] D.A. Korneev, V.I. Bodnarchuk, V.F. Peresedov, V.V. Zhuravlev and A.F. Schebetov, *Physica B* **276** 314 (2000).
- [8] V.I. Bodnarchuk Thesis, FLNP at JINR/Dubna (2003).
- [9] M. De Jong, J. Sietsma, M.Th. Rekveldt, B.P. Toperverg, V.V. Deriglazov, V.V. Runov, A.I. Okorokov, H. Eckerlebe and R. Kampmann, *J. Non-Crystalline Solids* **205–207** 645 (1996).
- [10] M. De Jong, Thesis, Delft University of Technology (1996).
- [11] B.P. Toperverg, *JETP Lett.* **37** 496 (1983); B.P. Toperverg, V.V. Deriglazov, V.E. Mikhailova, *Physica B* **183**, 326 (1993).
- [12] A.I. Okorokov, V.V. Runov, B.P. Toperverg, A.D. Tret'yakov, E.I. Mal'tsev, I.M. Puzei and V.E. Mikhailova, *JETP Lett.* **43** 503 (1986).
- [13] <http://www.jinr.ru>
- [14] S.K. Sinha, E.B. Sirota, S. Garoff and H.B. Stanley, *Phys. Rev. B* **38** 2297 (1988); B.P. Toperverg, *Physica B* **297**, 160 (2001).
- [15] V. Lauter-Pasyuk, *et al.*, *Phys. Rev. Lett.* **89** 167203 (2002).
- [16] V. Lauter-Pasyuk, B. Toperverg, M. Jernenkov and H. Lauter, *ILL Ann. Report* **2004** 108 (2005).
- [17] H. Lauter, B.P. Toperverg, V. Lauter-Pasyuk, A. Petrenko and V. Aksenov, *Physica B* **350**(Suppl. 1) E759 (2004).
- [18] B.P. Toperverg, H.J. Lauter and V.V. Lauter-Pasyuk, *Physica B* **356** 1 (2005).